THE JOURNAL OF PHYSICAL CHEMISTRY B

Article

pubs.acs.org/JPCB

Insight into the Structure of Photosynthetic LH2 Aggregate from Spectroscopy Simulations

Olga Rancova,*[,†] Juozas Sulskus,[†] and Darius Abramavicius*[,†,‡]

[†]Department of Theoretical Physics, Vilnius University, Saulėtekio al. 9-III, LT-10222 Vilnius, Lithuania

[‡]State Key Laboratory of Supramolecular Structure and Materials, Jilin University, 2699 Qianjin Street, Changchun 130012, PR China

Supporting Information

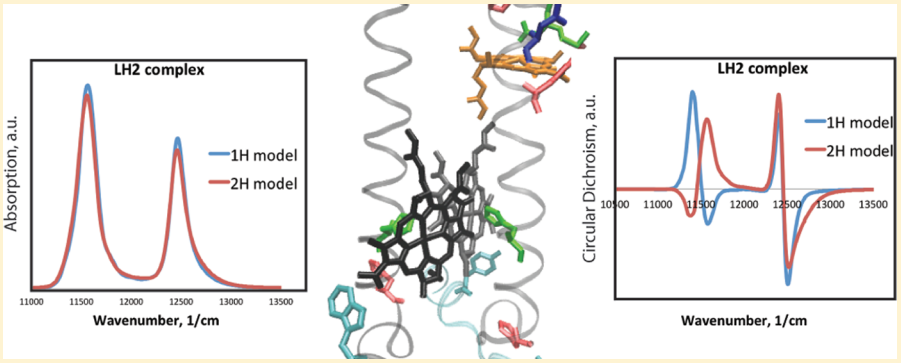

ABSTRACT: Using the electrostatic model of intermolecular interactions, we obtain the Frenkel exciton Hamiltonian parameters for the chlorophyll Q_y band of a photosynthetic peripheral light harvesting complex LH2 of a purple bacteria *Rhodopseudomonas acidophila* from structural data. The intermolecular couplings are mostly determined by the chlorophyll relative positions, whereas the molecular transition energies are determined by the background charge distribution of the whole complex. The protonation pattern of titratable residues is used as a tunable parameter. By studying several protonation state scenarios for distinct protein groups and comparing the simulated absorption and circular dichroism spectra to experiment, we determine the most probable configuration of the protonation states of various side groups of the protein.

INTRODUCTION

Photosynthetic apparatuses of bacteria and higher plants are the objects of investigations of scientists from diverse areas trying to understand the structure and underlying mechanisms of the highly effective natural solar energy converters.[1,2] As more precise structures of photosynthetic complexes become available, there appear more possibilities to explore their spectral properties and excitation dynamics obtained directly from the structural data. The aim of such studies is to reveal the roles of different parts of the complexes in optimizing the efficiency of the light harvesting and excitation energy transfer within the particular complex and between the complexes to the reaction center.

In general, the bacterial photosynthetic apparatuses are simpler than those of the higher plants and often serve as trial models. One of such systems is the photosynthetic peripheral light harvesting complex 2 (LH2) of purple bacteria, which is distinguished by an extremely red-shifted absorption band and highly symmetric structure.[3−5] The near-IR absorption spectrum of the LH2 complex of *Rhodopseudomonas acidophila* (now *Rhodoblastus acidophilus*[6]) strain 10050 is generated by the Q_y transitions of the bacteriochlorophyll *a* (BChl) molecules. These molecules are organized in two rings, named B800 and B850 by their lowest absorption wavelength at room temperature. The overall structure of the complex is cylindrical, characterized by C_9 symmetry with two transmembrane proteins α and β, both sequenced,[7] three BChl *a*, and either one or two carotenoid molecules per symmetric unit[8−10] (see Figure 1). Nine BChl molecules are distributed rather sparsely composing the B800 ring close to the cytoplasmic surface of the membrane, whereas 18 BChls of the B850 ring on periplasmic side are densely packed. The B850 ring is made of dimeric BChl units,[11] one bound to the α-protein, another to the β-protein.

The absorption spectrum of the LH2 complex in the region of Q_y transitions of the BChls at 77 K has two clear sharp distinct peaks[13] with maxima positioned at 801 nm (B800 band) and 867 nm (B850 band), with full-widths at half-maximum of 11 and 22 nm, respectively, and the ratio of B850 maximum with respect to B800 maximum equals 1.16. The contribution of the particular groups of pigments into producing this spectrum are defined rather well.[13,14] The recent femtosecond coherent experiments reveal more details on the excitonic interactions in the LH2[15] and similar LH3[16]

Received: March 24, 2012
Revised: May 23, 2012
Published: May 31, 2012

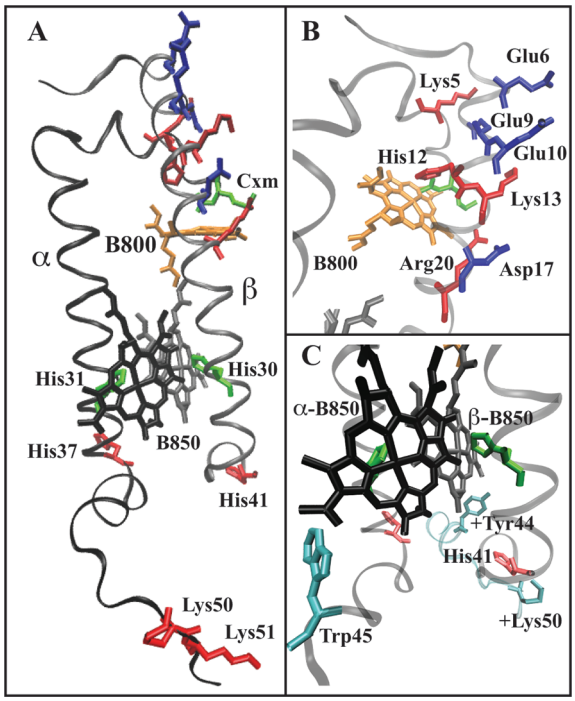

Figure 1. (A) LH2 symmetric unit: α-protein - dark gray; β-protein - light gray; α-B850 BChl - dark gray; β-B850 BChl - light gray; B800 BChl - orange; BChl Mg atom ligands - green; amino acids with positively charged side-chains - red; amino acids with negatively charged side-chains - blue; H-bond donors - cyan. (B) B800 area. (C) B850 area. The residues are marked in PDB notation. The "+" sign denotes the residue of the adjacent symmetric unit. Created with VMD.[12]

aggregates. The experiments reveal the evidence of quantum mechanical interference, which represents a previously undescribed strategy for control of excitonic dynamics as revealed by the phase map of quantum beating signals in the two-dimensional signals of the LH2.

Since the first crystallographic structure of the LH2 complex of *Rhodopseudomonas acidophila* was published,[8] there have been numerous studies performed, often combining experiments with theoretical modeling, seeking to connect structural properties with functions of the complex (see, for example, refs 11, 13, 14, and 17−23). Other purple bacteria belonging to the same type as *Rhodopseudomonas acidophila*, or to another type (with types distinguished based on the position and lineshapes of their spectra[13]) have been intensively studied as well.[3−5] However, a direct link between the microscopic structure and the spectroscopic data has not yet been established. The present paper describes the implementation of the structure-based electrostatic model seeking to quantitatively reproduce the spectral properties of the LH2 complex.

Theoretically, the light absorption and emission properties of the photosynthetic pigment−protein complexes can be described using the Frenkel exciton model.[2,24] Some parameters of this model can be related with the electrostatic properties of the complexes.[25] In the present research we employed the approach adapted from methods described in refs 26−29. These methods were developed based mainly on the treatment of structural data of the Fenna−Matthews−Olson antenna complex of green sulfur bacteria[30] and later applied to investigate other more complicated photosynthetic complexes such as PSI,[31] LHCII,[32] and others. The results of these studies confirm the efficiency of the developed methods.

Despite numerous experimental and theoretical publications revealing structural and spectroscopic properties of photosynthetic complexes, there are still open questions in connecting some of their structural peculiarities with the functional characteristics. One of the problems in implementing the microscopic methods for parametrization of the Frenkel exciton Hamiltonian is the precise characterization of charge distribution within the complex, which is necessary for correct estimation of certain excitation energies of pigments. The structural data of photosynthetic aggregates do not contain hydrogen atoms, and it is a nontrivial task for a researcher to identify possible protonation states of amino acids or to determine hydrogen-bonds within molecular complexes. Several numerical algorithms are developed to predict these data (see, for example, refs 33 and 34). However, the extended interaction networks between protein groups in the photosynthetic complexes often make the determination of protonation states difficult and ambiguous.

In this paper we present a different approach in solving this problem, which is based on the direct comparison of the simulated spectral properties of LH2 complex[13] to the corresponding experiments, serving as a benchmark of the microscopic simulation model, thus determining the charged states of amino acids or other charge distributions within the complex under investigation. The general idea is to make a straightforward connection from structural data to the spectral properties avoiding any additional modeling in between. In the original methods,[26−29] the hydrogen atoms are modeled explicitly, and the protonation states of the titratable residues are either assumed to be as in a solution with pH 7 (standard protonation pattern)[26,29] or obtained from electrostatic energy calculations.[31] In the present research we do not model hydrogen atoms explicitly except for hydrogen-bond donors to pigment molecules. We explore the protonation pattern of the complex as a tunable parameter (based on the standard protonation states of the titratable residues), which is fitted with respect to the optical spectra of the complex.

Our approach thus involves not only the ab initio modeling, but also simulations of excitonic spectra, while comparison with experiments allows adjustment of the initial structural information. Thus, making only general assumptions about the electrostatic interactions within the LH2, we examine the significant parts of the aggregate, which shape the experimentally known excitonic spectra.

METHODS

The Electrostatic Model of the Frenkel Exciton Hamiltonian. The light absorption and emission properties of the photosynthetic aggregates are described using the Frenkel exciton Hamiltonian. In the representation of pigment excitations, it is given by[2,24,25,35]

$$\hat{H} = \sum_{m} E_m \hat{B}_m^{\dagger} \hat{B}_m + \sum_{mn}^{m \neq n} V_{mn} \hat{B}_m^{\dagger} \hat{B}_n \qquad (1)$$

Here $\hat{B}_m^{\dagger}$ is the creation operator of an excitation on pigment m, while $\hat{B}_m$ is the conjugate annihilation operator. V_{mn} is the interpigment coupling. E_m is the pigment excitation energy in the aggregate, which is the main characteristic of the pigment and includes electrostatic properties of the environment as well.

dx.doi.org/10.1021/jp302817p | J. Phys. Chem. B 2012, 116, 7803−7814

The values of the Frenkel exciton Hamiltonian elements are defined by the electrostatic interactions between the pigments and their environment in the pigment−protein complex. If the atomic structure is known, these can be calculated from a structural models by assigning partial charges to the atoms of the pigment molecules and the protein molecules. The excitonic parameters are given by the Coulomb coupling between these charges. The polarization effects of the environment are taken into account through the effective dielectric constant, which is responsible for the screening of the electrostatic interactions.

The site-energy of the pigment E_m in the pigment−protein complex is the transition energy of the complex when that molecule is being excited. The local environment induces the shift in the pigment transition energy compared to the one it has in vacuum. We denote the vacuum phase pigment transition energy as E_0. The site-energy is then given by

$$E_m = E_0 + \Delta E_m \tag{2}$$

In this case, the site-energy shift ΔE_m needs to be evaluated, while E_0 is assumed to be the same for all identical pigments within the complex. Since E_0 is usually not available, it may be used as a parameter to set the absolute position of the spectrum and may be estimated from experiment.

Our calculations are based on the methods developed in refs 26−29 and summarized in ref 36. In the present research we adapt the charge density coupling (CDC) method[29] to calculate the site-energy shifts of the pigments. The transition charge from electrostatic potential (TrEsp) method[27] is used to calculate the excitonic couplings.

The pigments that are responsible for light absorption are identified, all other molecules create the background charges. Three types of atomic partial charges are used for the pigments. One set of charges describes the pigments in their equilibrium ground state. We denote this set by $q^{(00)}_{(I,m)}$; the subscript (I,m) denotes the Ith atom within the mth pigment. The next set defines the change of the charge distribution of the pigment when it is transferred from the ground into the excited state. The elements of this set are $\Delta q_{(I,m)} = q^{(1,1)}_{(I,m)} - q^{(0,0)}_{(I,m)}$. Here $q^{(1,1)}_{(I,m)}$ is the set of partial charges of the chromophore in its excited state. The third type of partial charge, $q^{(1,0)}_{(I,m)}$, describes the transition charge density of molecule m. It is a characteristic of the optical transition. All these partial charges are obtained by fitting the ab initio calculated electrostatic potentials of the ground and excited states of the pigments.[27]

The background charges of surrounding molecules, which are not optically active, are characterized only by their ground state charge distribution. The partial charges on the Jth atom of the kth background molecule is denoted by $q^{(bg)}_{(J,k)}$. Using this notation, the site-energy shift of the mth pigment of the pigment−protein complex is calculated as follows:

$$\Delta E_m = \frac{1}{\varepsilon_{\text{eff}}} \sum_{I=1}^{N} \sum_{k=1}^{M} \sum_{J=1}^{K} \frac{\Delta q_{(I,m)} \cdot q^{(bg)}_{(J,k)}}{|\mathbf{r}_{(I,m)} - \mathbf{r}_{(J,k)}|} \tag{3}$$

where N is the number of partial charges of the mth pigment molecule, M is the number of background molecules, K is the number of the partial charges of the kth background molecule, and $\mathbf{r}_{(I,m)}$ is the coordinate of the Ith atom of mth molecule. The effective dielectric constant ε_{eff} reflects the polarization and screening effects of the environment within the pigment−protein complex. The site-energy shifts (eq 3) are then used to calculate the site-energies (eq 2).

The excitonic couplings between the pigments V_{mn} are given by the electrostatic interaction of the atomic partial charges representing the transition densities of the pigments:

$$V_{mn} = \frac{1}{\varepsilon_{\text{op}}} \sum_{I=1}^{N} \sum_{J=1}^{N} \frac{q^{(1,0)}_{(I,m)} \cdot q^{(1,0)}_{(J,n)}}{|\mathbf{r}_{(I,m)} - \mathbf{r}_{(J,n)}|} \tag{4}$$

Here, similar as in eq 3, the summations run through all the atoms of mth and nth pigment molecules with partial charges assigned, whereas ε_{op} denotes the optical dielectric constant.

We apply the above-mentioned approach to the LH2 complex of the purple bacteria *Rhodopseudomonas acidophila*. However, in order to calculate the elements of the exciton Hamiltonian, the following data has to be ready: (1) the structural data on the pigment−protein complex containing the atomic coordinates of the molecules within the complex, (2) the sets of atomic partial charges for the pigment molecules, (3) sets of background partial charges, and (4) the effective dielectric constants ε_{eff} and ε_{op}. The important difference between our approach and the original CDC method lies in the determination of the last two items, namely, background charges and dielectric constants of the pigment−protein complex. All of this is discussed further.

For the LH2 complex of the purple bacteria *Rhodopseudomonas acidophila* strain 10050 of interest, the structural data obtained by X-ray diffraction are available in two entries in the Protein Data Bank (PDB): 1KZU[9] at 2.5 Å resolution and 1NKZ[10] at 2.0 Å resolution. We used the latter in our research, as its resolution is finer. Unlike in the 1KZU[9] structure file, there are two carotenoid molecules unraveled in 1NKZ[10] structural data. However the interpretation of the second carotenoid was strongly questioned.[37] Nevertheless, we used the structural data from the 1NKZ entry as it is.

The biological assembly of the LH2 of *Rhodopseudomonas acidophila* is a nonamer. The PDB entry 1NKZ contains an asymmetric unit composed of three protomer complexes with nine BChl molecules and six apoproteins in total. Three copies of the unit generated applying translation and rotation transformation compose the complete nonamer representing the LH2. Therefore only 1/3 of the Frenkel exciton Hamiltonian parameters calculated using these structural data are unique.

For modeling of pigments we use the partial charge sets of the Q_y transition of the BChl *a* molecules as given by Madjet et al.[27] calculated by the TDDFT/B3LYP method. The partial charges are situated only on bacteriochlorin rings with Mg atoms in the center. The phytyl tails are left uncharged and are not included in the calculations.

The absolute magnitude of charges have to be normalized to some observables.[27] Madjet et al.[27] normalized charges according to the empty cavity vacuum dipole moment magnitude of 6.1 D for a BChl *a* molecule as published in ref 38, whereas a larger vacuum dipole strength of 6.6 D for a BChl *a* is reported in the same paper as well. The authors of another study exploring the electronic relaxation in LH2 of a different purple bacterium *Rhodospirillum molischianum*[39] have scaled the charges to match the experimental value of the dipole moment of 6.3 D taken from ref 17. The scaling factor should therefore be considered as an adjustable parameter. In the present research, we use a somewhat different strategy for scaling the ab initio calculated atomic partial charges discussed in the next section.

The next issue to be defined is the characterization of background charges within the LH2 complex. The background is considered to be of five different types in the LH2: (1) the pigments not involved in the optical transition event, (2) the carotenoid molecules, (3) the backbones of the proteins, (4) the hydrogen-bonds, and (5) the protein side-chains and termini. Here the groups labeled 1−4 are generally neutral with atomic partial charges reflecting only dipole polarizations within the molecule. Thus we describe modeling of these background charges briefly in the following subsection. The background elements (5), the charged side-chains of proteins and their N- and C-termini, are our main focus.

Modeling of the Charge-Neutral Background. *Pigments Not Involved in the Optical Transition Event and Carotenoid Molecules.* Since the energy of the *m*th pigment molecule is shifted by all surrounding charges, the other pigment molecules being in their ground states have to be treated as the background. Their atomic partial charges are used as given in ref 27, but are additionally rescaled as described later.

The atomic partial charges for the ground state of the carotenoid rhodopin glucoside of the complex have been calculated using ab initio quantum chemistry simulations. The ground-state geometry optimizations were performed using the DFT method[40] with hybrid B3LYP functional.[41] The standard 6-31G(d,p) basis set was used as implemented in the electronic structure modeling suite Gaussian 03.[42] During calculations, the influence of solvent or surrounding environment was not accounted for. At the same level, achieved electronic charge densities were used to assign the electrostatic potential derived point charges to all atoms of investigated structures. Atomic charges were fitted to reproduce the molecular electrostatic potential (MEP) at more than 4300 points around the molecules by the Merz−Singh−Kollman (MK)[43] scheme. Finally, only heavy atoms were assigned point charges by adding the charges of hydrogen atoms to chemically connected heavy atoms.

The obtained atomic partial charges for the ground state of the carotenoid rhodopin glucoside are given in the Supporting Information. In the present research we include two carotenoids per symmetric unit of the complex as they are presented in structural file 1NKZ.pdb.

Backbones of the Proteins. For the partial charges of the protein backbone, we adapted the atomic partial charges from the CHARMM package.[44] These partial charges are set on five atoms of protein backbone, namely C, O, HN, N, CA (PDB notation). However, the hydrogens are not available from X-ray data. It is possible to simulate their positions using a range of molecular modeling software; however, we choose to reduce the information content, and instead we map the partial charges of CHARMM onto four directly available atoms: C, O, N, CA. The charges are set so that the total dipole moment of the planar COH_NNC_A group is conserved. The obtained charge values are as follows: C + 0.5696, O − 0.6556, N + 0.0852, CA + 0.0006.

Hydrogen-Bonds. The hydrogen-bonds to BChl molecules have also static dipole moments. According to Papiz et al.[10] the hydrogen-bond donors are an α-Trp45 NE1 atom bonding to the OBB atom of α-B850 BChls, an α-Tyr44 OH atom bonding to the OBB atom of β- B850 BChls, a β-Arg20 NE atom and NH2 atom both bonding to the OBB atom of B800 BChls. We put a negative charge $-\delta_{(H)}$ at the atom that is a hydrogen-bond donor and a positive charge of the same magnitude to represent the hydrogen atom at 1 Å distance from this atom toward the atom indicated as a bond acceptor. The value of $\delta_{(H)}$ is used as a fitting parameter, but it is kept in the range reported by refs 45 and 46.

Modeling of Dielectric Environment. The electrostatic interaction between the pigments and with the protein background of the complex is screened by the polarization of the environment.[47] The dielectric constants are presented in both eq 3 for the site-energy shift and eq 4 for the exciton coupling to take into account the polarization effects. While the screening effects in the pigment−protein coupling (eq 3) can be described effectively by the static dielectric constant, the excitonic coupling (eq 4) is screened only by the fast (optical) polarization of the environment. For excitonic couplings, there have been studies performed seeking to obtain the universal formula for the distance dependence of the screeing effects in exponential form as in refs 48 and 49. Although the empirical distance-dependent screening function was proposed there, they also concluded that medium effects are strongly dependent on the particular light-harvesting system considered. An alternative approach for treatment of the excitonic couplings in the dielectric media[50] concluded that screening effects depend on the mutual orientation of the pigments and on the dielectric boundaries rather than on distance. On the other hand, at short distances, the static dielectric constant loses its explicit meaning since the medium is not continuous. Additionally, on a microscopic scale, the medium of the pigment−protein complex is not known exactly. Thus, in the present article we assume the dielectric constant to be at the level of the effective screening and treat it as a fitting parameter.

The value $\varepsilon_{op} = 1$ is used in eq 4 for excitonic coupling. The atomic transition partial charges of BChls[27] are then scaled to get the experimentally confirmed value of the nearest neighbor excitonic coupling. In our approach, the scaling factor of BChl atomic partial charges reflects not only the dipole moments of the optical transition of the molecules but also the screening of the medium between them. We apply the same scaling factor in eq 3 for the BChl atomic partial charges of the ground and excited states for the same reason.

The value $\varepsilon_{eff} = 1$ is used for the electrostatic interactions of pigments with the charged amino acid side-chains that are ligands of the BChl Mg atom, and with the atomic partial charges representing hydrogen-bonds between proteins and pigments (i.e., for the charges separated by less than 3 Å) in the calculation of the site-energy shifts in eq 3. The value of $\varepsilon_{eff} = 1.2$ is used in other cases.[13]

Modeling of Charged Protein Side-Chains and Termini. The protonation states of titratable residues in protein depend on pH of the environment and other neighboring charges (see, for example, ref 51). The absence of the hydrogen atoms in the structural data files leaves the protonation states undetermined. In the original CDC method, the protonation states of the titratable residues are either assumed to be standard[29] (as in a solution with pH 7) or obtained from electrostatic energy calculations,[31] whereas we use the protonation pattern of the complex as a tunable parameter based on the standard protonation states. Under physiological conditions, it is known that arginine and lysine should be positively charged, and aspartic acid and glutamic acid should be negatively charged, while histidine side-chains with its imidazole ring have several protonation options, which are very sensitive to the nearest surrounding.[52] In our model, we put a negative or positive charge directly on the non-

hydrogen atom expected to be deprotonated or protonated. In all cases, when the residue has a resonance structure, we redistribute the putative charge to describe delocalized electrons. Thus, because of the conjugation between the double bond and the nitrogen lone pairs in the guanidinium group of arginine, the positive charge is delocalized, and we assign the partial charges of +0.33*e* to all three nitrogen atoms NE, NH1, and NH2 (see Figure 2a). The histidine side-chain

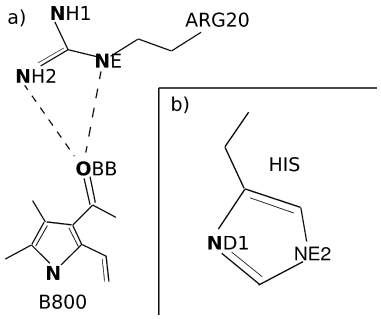

Figure 2. (a) Schematic representation (not to scale) of the close contacts between the side-chain of β-Arg20 residue and the B800 BChl molecule at its OBB atom. (b) Structure of histidine residue side-chain. The atoms are marked in PDB notation. Dashed lines mark hydrogen-bonds.

has two nitrogen atoms within the imidazole ring (see Figure 2b), which can be double protonated (positively charged side-chain), single protonated (neutral side-chain), and in rare cases double deprotonated (negative side-chain). Due to the two resonant structures of the histidine with the imidazole ring, we assign partial charges of +0.5*e* to both nitrogen atoms ND1 and NE2 of the ring when the group is positively charged, or partial charges of −0.5*e* to these atoms when the group is negatively charged, and zero charges to both atoms when the group is neutral. Similarly, we distribute the −0.5*e* partial charges on oxygen atoms of negatively charged carboxyl groups.

RESULTS

Distinct Contributions to the Hamiltonian. In this section we describe how the Hamiltonian parameters depend on the possible microscopic structural arrangement, and later relate these to the experimental spectra. The calculated values of the Frenkel exciton Hamiltonian of LH2 complex reflect its symmetric structure. As follows from the 1NKZ file described above, only 1/3 of the values calculated from the structural data are unique. Thus we present only the values for 6 BChl *a* molecules of the B850 ring and 3 BChl *a* molecules of the B800 ring. In the following, the BChl molecules are denoted as in 1NKZ.pdb file, i.e., BChls 301, 303, 305 belong to the α-bond B850 subring, 302, 304, and 306 belong to the β-bond B850 subring, and BChls 307, 308, and 309 belong to the B800 ring. The proteins of chains A, C, and E are α-peptides of the inner ring of the complex, and proteins B, D, and F are β-peptides of the outer ring of the complex.

We first estimate the interpigment couplings since they depend only on the BChls. It has been shown by experiments and modeling[13,14,17] that the Q_y transition of B850 BChls participates in the creation of both 800 and 850 nm components of the absorption and circular dichroism (CD) spectra. This points to the nearest-neighbor excitonic interactions within the B850 ring being ≈250−300 cm^{-1}. In the microscopic model, this value is directly related to the atomic partial charges of BChl due to eq 4, which can be used to rescale the charges. We used the nearest-neighbor coupling for rescaling the ab initio atomic partial charges of BChl *a* molecules seeking to reproduce the mentioned value.

According to eq 4, BChl atomic partial charges[27] rescaled by 0.732[39] with $\varepsilon_{\text{eff}} = 1$ produce the nearest-neighbor coupling in the B850 ring of 224 cm^{-1}, which is slightly undervalued compared to those of the spectroscopic studies (≈250−300 cm^{-1}). We choose the rescaling factor 0.81, which gives the nearest-neighbor coupling ≈273 cm^{-1} and guarantees correct excitonic splitting in the spectrum. Notice that in such approach the scaling factor also includes the screening effects of the environment.

The excitonic couplings are then as follows: couplings of the B850 ring pigment with its nearest neighbors are 271−276 cm^{-1} within a dimer and 224−228 cm^{-1} with the nearest neighbor from the adjacent dimer; couplings of the α-B850 subring pigment with its nearest neighbors in the subring are −70 cm^{-1}; couplings of the β-B850 subring pigment with its nearest neighbors in the subring are −47 to −48 cm^{-1}; couplings between nearest neighbors within the B800 ring are −33 to −34 cm^{-1}; and couplings between nearest pigments from different rings are ∼34 cm^{-1}. All other excitonic couplings are much weaker and could be neglected.

The site-energy shifts of the pigments are calculated from eq 3. Since the equation is additive with respect to various charged groups, we study separately the effects of background pigments, carotenoids, protein backbone, and its side groups.

First, we evaluate the influence of background BChls on the site-energy shift of the particular pigment molecule. The obtained site-energy shifts are presented in Table 1, where the

Table 1. CDC Calculated Site-Energy Shifts (in cm^{-1}) Caused by B850 and B800 Ring Pigments, Protein Backbones, and Carotenoids

site	B800	B850	A	B	C	D	E	F	Car	total
301	8	110	55	−35	−40	−7	1	1	−8	84
302	−2	123	3	2	−61	33	4	−2	−2	99
303	8	108	5	1	54	−40	−42	−8	−7	80
304	−2	120	3	−2	6	−2	−62	33	−1	94
305	8	107	−41	−8	3	2	58	−35	−5	90
306	−2	117	−61	33	3	−2	7	0	−0	96
307	−7	1	114	18	11	10	−9	−0	−3	135
308	−7	1	−9	−0	112	21	12	10	−3	136
309	−7	1	11	9	−8	−0	112	19	−3	133

dx.doi.org/10.1021/jp302817p | J. Phys. Chem. B 2012, 116, 7803−7814

Table 2. CDC Calculated Site-Energy Shifts (in cm^{-1}) Caused by Terminal Parts of Proteins of Chains A–F: *N* - Charged N-Terminus; *C* - Charged C-Terminus

	A		B		C		D		E		F		
site	*N*	*C*	*N*	*C*	*N*	*C*	*N*	*C*	*N*	*C*	*N*	*C*	total
301	−4	−4	−7	−60	−14	−7	−8	7	1	4	−8	31	−69
302	−2	−14	3	−27	−4	−4	2	26	8	−4	3	−24	−37
303	0	4	−8	29	−4	−3	−7	−59	−14	−7	−9	7	−71
304	8	−4	3	−24	−2	−14	3	−27	−4	−3	2	27	−35
305	−14	−7	−8	7	0	4	−8	30	−4	−3	−7	−61	−71
306	−4	−3	2	26	8	−4	3	−24	−2	−14	3	−32	−41
307	118	2	10	7	34	1	15	−5	−23	−1	9	1	168
308	−24	−0	9	2	129	2	10	8	33	1	15	−5	180
309	33	1	14	−5	−24	−0	8	2	112	2	10	8	161

Table 3. CDC Calculated Site-Energy Shifts (in cm^{-1}) Caused by Charged Amino-Acid Side-Chains

site	Arg	Lys	Asp	Glu	His 12	His 37	His 41
301	−16.73	−4.50	17.02	41.35	−21.65	−92.31	13.51
302	−1.09	31.30	−0.68	−5.09	7.19	141.94	27.93
303	−17.40	−1.12	17.71	43.75	−22.96	−92.57	13.06
304	−1.11	28.09	−0.63	−3.66	6.21	136.95	28.45
305	−16.91	−0.57	17.31	42.04	−21.89	−88.15	12.49
306	−1.40	31.31	−0.20	−2.75	5.90	135.47	27.43
307	−656.65	14.68	19.54	−105.08	91.98	8.78	−2.28
308	−676.65	34.62	22.25	−105.77	95.70	6.92	−3.21
309	−665.02	35.86	23.10	−106.70	90.73	7.42	−2.75

columns "B800" and "B850" contain energy shifts caused by all pigments of the B800 ring and the B850 ring, respectively. As seen in Table 1, the BChls of the B800 ring have minor influence on the site-energies of any pigments. That is expected taking into account the distances between the pigments within the ring and with the B850 ring. However, the densely packed B850 ring induces the total blue shift of ≈110–120 cm^{-1} of the B850 pigments. This is an unexpected result, as the B850 ring is known as the BChls system with one of the most red-shifted absorption bands.

Second, the column marked "Car" contains energy shifts induced by the two carotenoid rhodopin glucoside molecules per symmetric unit. The influence of both carotenoids on the site-energies of B800 BChls is not significant, whereas for site-energies of the B850 ring, the influence of one carotenoid is mostly canceled by another one with energy shifts in the range of ±10–20 cm^{-1}.

Third, the energy shifts caused by protein backbone of particular chains are shown in columns A–F of Table 1. As seen in Table 1, in general, protein backbones cause the down-shift of the site-energies of B850 ring pigments of ca. −25 cm^{-1} and raise the energies of B800 ring BChls by ≈145 cm^{-1}, which is of the same order of magnitude as the impact of the B850 ring on B850 pigments. The total impact of all mentioned groups of the complex on the site-energy shifts is listed in the last column of Table 1. The data reveals that these parts of the complex altogether do not produce any significant diversity of the site-energies of BChls.

Next we evaluate the impact of possibly charged protein termini on the site-energies of BChls. The terminal groups of polypeptide chains are considered as follows. The C-termini of both α and β proteins, which are identified as alanine and histidine amino-acids respectively, are deprotonated and negatively charged under the conditions expected in the photosynthetic antennas. Their influence is presented in the Table 2 columns denoted "*C*". Under similar conditions, N-termini can be protonated and positive. There is an alanine amino acid on the N-terminus of β proteins, whereas the methionine N-terminus of α proteins in the LH2 is modified by the carboxyl group forming N-carboxymethionine.[10] Data in Table 2 reveal that the charged N-terminus of α proteins (chains A, C, E) if protonated is important in raising the site-energy of B800 pigments compared to B850 ones, whereas the charged N-terminus of β proteins (chains B, D, F) has minor influence on the site-energies of both B800 and B850 rings, as this terminus is more distant. The total impact of charged terminal groups of proteins on the site-energies of BChls is listed in the last column of Table 2. Notice that the N-termini can be protonated (positive) or deprotonated (neutral), which is described in the Discussion and Conclusions section.

As seen from Tables 1 and 2, the proteins with charged termini play a major role in raising the site-energies of the B800 ring by nearly 275 cm^{-1} compared to the B850 ring, but only minor splitting of the energies of the B850 ring pigments is generated.

We next investigate the site-energy shifts caused by charged amino-acid side-chains of proteins. In the structural data of the LH2 complex, we consider the following residues as possibly charged: Lys5, Lys50, Lys51, and His37 (all positively charged) in the α-protein; Arg20, Lys13, His12, His41 (positively charged), Asp17, Glu6, Glu9, and Glu10 (negatively charged) in the β-protein (see Figure 1). Here we do not include the amino-acid side-chains that are ligands to Mg atoms of BChl molecules. Those are treated separately.

In the physiological environment characterized by pH = 7–8, arginine and lysine are protonated (positive), while aspartic

dx.doi.org/10.1021/jp302817p | J. Phys. Chem. B 2012, 116, 7803–7814

acid and glutamic acid are deprotonated (negative). However, under the same conditions, histidine can be either singly protonated and neutral or doubly protonated and positive. Thus we present the contributions caused by each histidine residue separately, while other charged amino acids are treated all together. The resulting site-energy shifts caused by charged side-chains are presented in Table 3. It shows that the charged arginine side-chain induces drastic red shift of the site-energies of the B800 ring compared to B850. It is remarkable that there is only one arginine amino acid per protomer in the LH2 complex. So it is not a collective influence, but rather the impact of a single residue placed at a crucial position.

The collective action of three negatively charged glutamic acid residues also creates a significant red-shift of site-energies of B800 pigments. However, this impact can be largely compensated if the His 12 residue is charged positively. This residue together with another possibly charged side-chain of His 37 induces appreciable energy splitting of B850 ring pigments.

Important contribution to the site-energy shifts originates from protein side-chains ligating Mg atoms in the center of bacteriochlorin rings (see Figure 1). The central Mg atoms of B850 ring BChls are coordinated by histidine residues of α- and β-proteins, namely α-His31 coordinates B850 BChl molecule of the same chain, and β-His30 coordinates B850 BChl belonging to adjacent chain. The BChls of B800 ring are coordinated by carboxyl group of modified N-terminus N-carboxymethionine (Cxm) of α-proteins. Ligands are expected to be anionic or charge-neutral. Even though negative state of the histidine side-chain is not usual, it is observed in some similar complexes of BChls and imidazoles.[53] The carboxyl group of N-carboxymethionine can be deprotonated as well. The possible influence of these negatively charged ligands on the site-energies of pigments molecules is shown in Table 4.

Table 4. CDC Calculated Site-Energy Shifts (in cm^{-1}) Caused by Ligands of the BChl Mg Atom and Hydrogen-Bonds to BChls

site	His 30	His 31	Cxm	H bond
301	231.43	60.19	18.84	−4.57
302	−159.07	51.93	−4.77	−5.18
303	228.32	26.01	20.06	−4.57
304	−177.49	52.03	−3.95	−5.18
305	227.02	49.87	19.09	−4.61
306	−183.25	57.00	−3.54	−5.19
307	0.79	−17.42	−130.83	−9.32
308	3.51	−14.46	−141.74	−9.77
309	2.57	−15.25	−136.03	−9.54

As seen in Table 4, the largest impact arises from the β-His30 negatively charged side-chain. It strongly influences both α- and β-bond BChls of the B850 ring, splitting their site-energies by nearly 400 cm^{-1}. This is not surprising, as this residue not only coordinates B850 β-BChls but also lies within the hydrogen-bonding distance of the keto group on ring E of the opposing BChl molecule. However, the angle is not favorable for the H-bond formation. On the other hand, another histidine ligand (α-His31) causes smaller shifts and very little splitting. In general, it down-shifts the energies of the B800 ring pigments and up-shifts the mean energy of the B850 ring pigments. *N*-Carboxymethionine ligand also remarkably down-shifts the energies of the B800 pigments it coordinates and, quite unexpectedly, also participates in splitting of the site-energies of the B850 ring. It is important to notice that negatively charged histidine ligands split the site-energies of the B850 ring pigments in an opposite way than the splitting produced by other charged parts of the LH2 complex listed in Tables 1, 2, and 3.

The last type of background charges we examine are due to hydrogen-bond donors to the pigment molecules, which are modeled as dipoles. The magnitude of the partial charge of the dipole $\delta_{(H)}$ can be used as a fitting parameter to reproduce the experimental absorption spectrum of Q_y transitions of the LH2 complex. However, the qualitative effect can be estimated here since the energy shift is directly proportional to the partial charge magnitude. Thus, we set a trial partial charge $\delta_{(H)} = 0.01e$, and the results are presented in the last column of Table 4. These trial values of the hydrogen-bond-induced site-energy shifts can be rescaled straightforwardly. It is necessary to mention that, unlike all other previously described background charges, the hydrogen-bonds to BChl molecules only induce a site-energy shift of the one particular pigment they are bound to.

As seen from the last column of Table 4, all hydrogen-bonds tend to red-shift the site-energies of the pigments. This is not surprising, as all these bonds are aimed at the same atom of BChl molecules, namely, the OBB atom of bacteriochlorin rings. The main difference arises from the fact that the OBB atom of B800 BChls has two hydrogen-bonds, whereas B850 pigments have only one bond each. It is clearly reflected in the values of site-energy shifts presented in Table 4.

Optimization of the Microscopic Charge Pattern. As described above, the X-ray structural data provides partial structural information (hydrogen atoms are still missing). The electrostatic data are even poorer: the partial charges must be rescaled, the hydrogen-bonds are approximate, the dielectric screening is approximate, and the protonation states of various protein side-chains are poorly defined. To obtain that missing information, we perform a search for the best set of parameters by using the spectroscopy data of the LH2 complex.[13] This allows to describe the impact of the particular charged side-chain on the site-energy shifts calculated from eq 3 and then to judge whether this configuration is acceptable from the spectroscopy viewpoint and to solve this problem unambiguously.

The spectroscopic parameters that fit the set of spectroscopy measurements have been nicely reviewed in ref 13. The Frenkel exciton Hamiltonian necessary for the modeling of the Q_y absorption spectrum of the LH2 complex of *Rhodopseudomonas acidophila* dictates the following: the site-energy splitting between the α- and β-bond chromophores of the B850 ring should be ∼300 cm^{-1}, and the difference between the site-energies of B800 pigments and the mean energy of B850 pigments is ∼336 cm^{-1}. After analyzing and combining the impacts of different parts of the LH2 complex on the site-energies of pigments in the previous section, we are able to propose two possible combinations of background charges that satisfy these conditions.

In general, we have the following: First of all, we are forced to state that the arginine amino acid side-chain must be deprotonated and neutral, even though the pK_a value of the separated amino acid is as high as 12.1. Otherwise, we do not find any justified ways to compensate the extreme down-shift it produces on the site-energies of B800 ring pigments compared

dx.doi.org/10.1021/jp302817p | J. Phys. Chem. B 2012, 116, 7803−7814

to B850 ones, as seen in Table 3. Second, the proposed terminal charged states presented in Table 2 help to approach the model of ref 13, and we accept them. Third, as follows from ref 10, there is a hydrogen-bond between the ND1 atom of the His41 residue and the NZ atom of the +Lys50 residue separated by only 2.86 Å (see Figure 1). These are exactly the atoms that could be protonated. In these circumstances, the protonation of His41 (so that it becomes positive) seems unlikely if we assume that all lysine residues, including Lys50, are protonated. We therefore decide to keep His41 in a neutral charge state. Another important hydrogen-bond, which involves the histidine side-chain, is the bond between the ND1 atom of His12 and the NE1 atom of the Trp7 residue. However, in this case we must keep His12 positively charged since it blue-shifts the energy of B800 ring pigments compared to B850 ones, as is necessary for the experimental data. Also, this does not place two positive charges at close proximity (like in the His41 case), as the tryptophan side-chain is assumed to be neutral.

In this perspective, one way to obtain reasonable parameters is to additionally assume that all amino acid side-chains listed in Table 3 except Arg and His41 are in their charged states. It gives us an energy splitting between the pigments of the B850 ring of ∼270 cm^{-1} and a site-energy difference between the mean values of the B800 and B850 rings of ∼250 cm^{-1}. The total site-energy shifts produced in this configuration are presented in the first column of Table 5 marked "(1)". Thus,

Table 5. CDC Calculated Total Site-Energy Shifts (in cm^{-1}) Caused by (1) Pigments of B800 and B850 Rings, Carotenoids, Protein Backbones, and Termini, Lys, Asp, Glu, His12, and His37 Charged Side-Chains; (1H) Same as (1) Plus H-Bonds ($\delta_{(H)}$ = 0.15; 0.01) (See Text); (2) Pigments of B800 and B850 Rings, Carotenoids, Protein Backbones and Termini, Lys, Asp, Glu, His12 Charged Side-Chains, and Charged His30 Ligand; (2H) Same as (2) Plus H-Bonds ($\delta_{(H)}$ = 0.2; 0.01) (See Text)[a]

site	(1)	(1H)	(2)	(2H)
301	−44.98	−113.57	278.76	187.31
302	237.00	159.37	−64.01	−167.52
303	−47.08	−115.68	273.80	182.34
304	224.80	147.14	−89.65	−193.18
305	−33.76	−102.98	281.40	189.11
306	224.30	146.49	−94.42	−198.17
307	332.14	322.82	324.15	314.83
308	369.69	359.91	366.28	356.51
309	343.83	334.29	338.98	329.44
Δ	255.17	318.88	245.49	333.61
$\delta_{(E)}$	−270.64	−261.75	360.68	372.54

[a] Δ = difference between the site-energy of the B800 ring and mean energy of the B850 ring; $\delta_{(E)}$ = site-energy splitting of the B850 ring.

the energy splitting of B850 ring pigments is rather satisfactory, but the energy difference between the rings is slightly too small. To relax this inconsistency, we use the flexibility of hydrogen-bond partial charges as parameters and set $\delta_{(H)} = 0.15e$ on hydrogen-bonds donated by α-Trp45 to α-B850 BChls and donated by α-Tyr44 to β-B850 BChls. Two hydrogen-bonds donated by β-Arg20 to B800 pigments are assumed to have $\delta_{(H)} = 0.01e$ (see discussion on different polarizations of hydrogen-bonds in the next section.) In this case, the hydrogen-bonding to B850 ring pigments down-shifts their site-energies by ∼69 cm^{-1} for α-bond pigments and ∼78 cm^{-1} for pigments bonded to the β-protein. The total site-energy shifts for such background charge arrangement are presented in the column of Table 5 marked "(1H)".

There is another possibility to obtain the site-energy values of LH2 pigments in agreement with ref 13. As discussed above, we keep all background charges as in Table 1 and Arg and His 41 side-chains uncharged. Further, we accept that side-chains of lysine, aspartic acid, and glutamic acid are charged as should be under physiological conditions. Also we keep the His 12 residue of β-proteins positively charged, seeking to compensate the down-shift of site-energies of the B800 ring caused by negatively charged glutamic acid side-chains, as seen from Table 3. With such background charge layout, the B800 ring site-energies are blue-shifted by ∼270 cm^{-1} compared to B850 ones, but B850 ring pigments are all of almost the same energy, with splitting of ∼40 cm^{-1} only. We then assume that the ligand of β-B850 BChls (the residue β-His30) is charged negatively and induces the energy splitting of B850 pigments as seen in Table 4. The total site-energy shifts caused by such background charge pattern are presented in Table 5 marked "(2)". As seen from these data, the splitting of site-energies within the B850 ring pigments of ∼360 cm^{-1} is quite satisfactory. However, the 245 cm^{-1} difference of mean site-energies between B800 and B850 rings is insufficient. Again the hydrogen-bond pattern allows us to lower the site-energies of B850 ring pigments. The values of partial atomic charges representing charge polarization of hydrogen-bond donors are $\delta_{(H)} = 0.2e$ for bonds with B850 ring pigments and $\delta_{(H)} = 0.01e$ for bonds with B800 ones. The total site-energy shifts of such a system are presented in the column of Table 5 marked "(2H)".

It is interesting to note that the mean site-energies of B800 and B850 ring pigments are rather similar in both cases (1H) and (2H), but the splitting of energies of B850 ring is the opposite, i.e., in the (1H) case, α-bond B850 pigments are of lower site-energy compare to β-bond ones, and in the (2H) case, vice versa. In this latter charge layout, the hydrogen-bonds to B850 pigments help in site-energy splitting of the α- and β-bond BChls of the ring, whereas, in the (1H) case, the site-energy splitting of B850 ring pigments is of opposite type, and the hydrogen-bonding decreases this splitting. The main role in B850 pigment site-energy splitting is played by differently protonated histidine amino acid side-chains. The α-His37 positively charged residue causes quite strong site-energy splitting of B850 ring pigments in the (1) case, but acts in the opposite way of ligand β-His30 if deprotonated and negatively charged in the (2) case (see Figure 1). Thus from our model it follows that only one of these residues can be in the charged state to create necessary site-energy shifts. This conclusion is supported not only by qualitative reasons. These residues are on the periplasmic side of the LH2 complex where the environment is expected to be apolar.

We thus find two models that provide qualitatively similar Hamiltonian matrices. In order to resolve this ambiguity, we simulate two spectroscopy experiments.

The simplest measurement is the linear absorption. The experimental absorption spectrum created by Q_y transitions of BChls[13] results in two peaks at 801 nm (≈12485 cm^{-1}) and 867 nm (≈11535 cm^{-1}) with a ratio of maxima B850/B800 equal to 1.16. According to the Frenkel exciton theory, the absorption spectrum is given by all possible transitions from the

dx.doi.org/10.1021/jp302817p | J. Phys. Chem. B 2012, 116, 7803−7814

ground state to the excited states scaled by their transition dipole amplitudes:[35]

$$\kappa_A(\omega) = \sum_e \langle |\mathbf{d}_e|^2 G_e(\omega)\rangle_\sigma \tag{5}$$

where $\langle ...\rangle_\sigma$ denotes the statistical averaging over the inhomogeneities, $\boldsymbol{d}_e = \sum_n \boldsymbol{\mu}_n \psi_{ne}$ is the transition dipole of exciton e; $\boldsymbol{\mu}_n$ is the transition dipole of pigment n, given by its partial charges

$$\boldsymbol{\mu}_n = \sum_{J=1}^{N} q_{(J,n)}^{(1,0)} \mathbf{r}_{(J,n)} \tag{6}$$

and ψ_{ne} is the exciton eigenvector obtained from the eigenequation

$$(E_m - \varepsilon_e)\psi_{me} + \sum_n^{m\neq n} V_{mn}\psi_{ne} = 0 \tag{7}$$

$G_e(\omega)$ in the absorption eq 5 is the spectral line shape function for exciton e:

$$G_e(\omega) = \mathcal{R}\int_0^\infty dt\, \exp[i(\omega - \varepsilon_e)t - g_e(t) - t/\tau_e] \tag{8}$$

$g_e(t)$ and τ_e are environment-related parameters.

The function $g_e(t)$ describes the homogeneous spectral broadening character of exciton e due to the coupling with the fluctuating environment. This effect is characterized by the spectral density function $C''(\omega)$ and the system-bath coupling parameter λ when the bath of all pigments is considered uncorrelated and identical. For simplicity we choose[35]

$$C''(\omega) = 2\lambda\frac{\omega\gamma}{\omega^2 + \gamma^2} \tag{9}$$

which then approximately gives

$$g_e(t) = \xi_{ee}\frac{\lambda}{\gamma}\left(\frac{2k_BT}{\gamma} - i\right)[\exp(-\gamma t) + \gamma t - 1] \tag{10}$$

where $\xi_{ee'} = \sum_n \psi_{ne}^2\psi_{ne'}^2$ is the exciton overlap parameter. The final ingredient is the exciton lifetime τ_e. It is the inverse of all possible exciton escape pathways. Using the Redfield theory for exciton transfer rates, we find[54]

$$\tau_e^{-1} = \sum_{e'}^{e'\neq e} \xi_{ee'}C''(\varepsilon_e - \varepsilon_{e'})\left(\coth\left(\frac{\varepsilon_e - \varepsilon_{e'}}{2k_BT}\right) + 1\right) \tag{11}$$

The static fluctuations of the environment (the conformational fluctuations) are included by adding the uncorrelated Gaussian diagonal disorder characterized by the width σ_e to the calculated energy shifts $E_m \rightarrow E_m + x$, where x is a random shift drawn from the Gaussian distribution. From the eigenvalue equation (eq 7) we find that the exciton eigenstate vectors ψ and eigenvalues ε become functions of x. All other properties, $g_e(t)$ and τ_e, now depend on the realization due to $\xi_{ee'}$. Numerical averaging over the disorder is thus performed to include the inhomogeneous broadening.

In the following, we present the absorption spectrum of the LH2 aggregate using the two sets of parameters obtained above. To obtain reasonable homogeneous and inhomogeneous line width parameters, we set γ^{-1} = 50 fs, λ = 120 cm^{-1}, σ = 37 (B800), and 190 (B850) adapted from ref 13, and we use 77 K temperature.

The site-energy shifts obtained in models (1H) and (2H) have been used to calculate the site-energies (eq 2) using E_0 = 12200 cm^{-1}. The absorption spectra of the LH2 complex obtained with these two sets of site-energies as parameters of Frenkel exciton Hamiltonian are shown in Figure 3. The

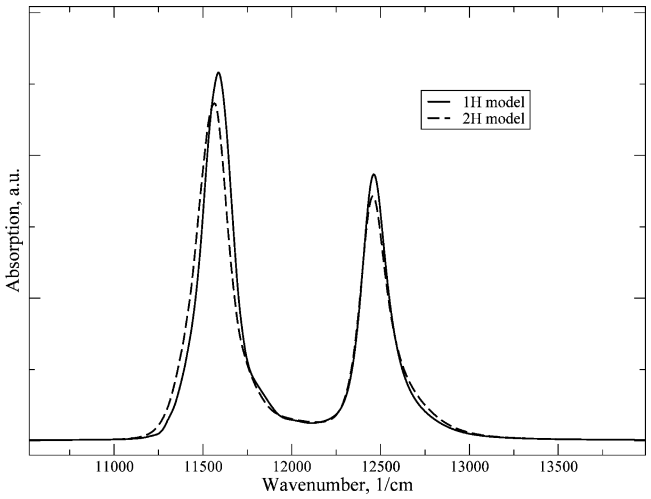

Figure 3. Linear absorption spectra of the LH2 complex obtained using site-energies of models (1H) and (2H) and described pigment–pigment excitonic couplings.

spectrum of the (1H) model (solid line) shows two main bands at ≈11590 cm^{-1} (B850 band) and ≈12460 cm^{-1} (B800 band), which produce a difference of 870 cm^{-1}, i.e., ≈80 cm^{-1} smaller than the experimental one, and a ratio of maxima B850/B800 of 1.38.

The absorption spectrum obtained employing the (2H) set of site-energies is shown by the dashed line in Figure 3. There are two bands as well: B850 at ≈11565 cm^{-1} and B800 ≈12455 cm^{-1}, with a difference of 890 cm^{-1} (≈60 cm^{-1} smaller that the experimental one) and a ratio of maxima B850/B800 of 1.38.

As seen from this figure, both sets of possible background charges of the LH2 complex lead to satisfactory absorption spectra. Thus, using only the absorption spectra as a benchmark, we cannot distinguish the substantial difference between two models and cannot resolve the underlying microscopic charge-pattern.

The CD spectroscopy, being sensitive to the chirality of the aggregates gives additional insight about the three-dimensional configuration of molecular geometry.[55] The CD spectrum is given by[56]

$$\kappa_{CD}(\omega) = \sum_e \langle \rho_e G_e(\omega)\rangle_\sigma \tag{12}$$

where

$$\rho_e = \sum_{mn} (\boldsymbol{\mu}_n \times \boldsymbol{\mu}_m)\cdot\mathbf{R}_{mn}\psi_{me}\psi_{ne} \tag{13}$$

is the rotational strength of the excitonic transition, and $\mathbf{R}_{mn}$ is the radius vector connecting the center of charge of pigments m and n. The center of charge of a BChl is taken as the center of mass of nitrogens NA, NB, NC, and ND.

The experimental CD spectrum[13] of LH2 of *Rhodopseudomonas acidophila* strain 10050 consists of two pairs of lines with the signature pattern − + + −. The lines in the B850 region are quite symmetric, with a zero crossing ≈6 nm red-shifted with

dx.doi.org/10.1021/jp302817p | J. Phys. Chem. B 2012, 116, 7803–7814

respect to the B850 absorption maximum. The simulated CD spectra for both models (1H) and (2H) are given in Figure 4.

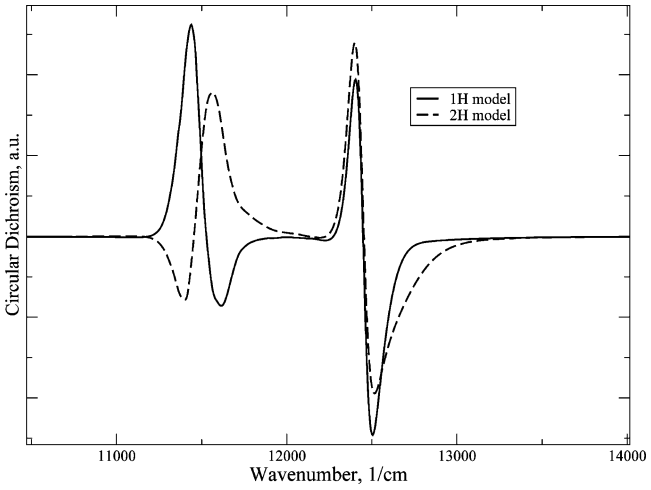

Figure 4. CD spectra of Q_y transitions of LH2 complex obtained using site-energies of models (1H) and (2H) and described pigment–pigment excitonic couplings.

They show that the (1H) background charge layout leads to a wrong pattern in CD spectrum (Figure 4, solid line), i.e., the calculated signature pattern appears to be − + − + going from the blue to the red region. However, the CD spectrum modeled with the (2H) background charges (Figure 4, dashed line) demonstrates the same signature pattern as the experimental spectrum.[13] The zero crossing in the B850 band region of this calculated CD spectrum is at ≈11455 cm^{-1}, i.e., red-shifted by nearly 110 cm^{-1} compared to the maximum position of B850 absorption band (Figure 3 dashed line), that corresponds to experimental redshift of this zero crossing of ≈6 nm. These results show that the (2H) background charge layout reproduces the spectral characteristics of the LH2 complex.

DISCUSSION AND CONCLUSIONS

We were able to obtain the absorption and CD spectra of the LH2 complex of purple bacteria *Rhodopseudomonas acidophila* strain 10050 presented in Figures 3 and 4 in remarkably good qualitative agreement with the main features of the experimental data.[13] This demonstrates that our rather simple model based on methods developed in ref 26–29 and on the structural data of the complex obtained by X-ray diffraction[10] allows one to quantitatively reconstruct the pattern of electrostatic fields inside the LH2 complex. In this section, we review the main assumptions made within the model.

The methods of calculations of parameters of Frenkel exciton Hamiltonian used here are not the only ones developed by the authors of refs 26–29, but are rather the most straightforward ones to apply. There are more sophisticated methods presented in the mentioned publications. Nevertheless, it has to be pointed out that all electrostatic models are approximate and induce errors. When more layers of electrostatic simulations are included, the errors are accumulated, and the accuracy of the obtained results becomes questionable. We thus use the simple electrostatic model, which can be easily coordinated with specific experiments by adjusting the tunable structural parameters. This general idea allows a straightforward connection of structural data and spectral properties, avoiding any additional modeling in between. Thus, making only general assumptions about the electrostatic interactions within the pigment–protein complex under investigation, our model allows one to determine the most important protein groups in generating the experimentally known spectra.

The structural parameter that we choose to vary is the charge distribution (protonation states of protein side groups) within the aggregate. It could be argued that the pH of an environment defines the protonation states; however, the heterogeneous structure of the photosynthetic aggregate does not provide a uniform environment for all protein groups. We believe that our approach provides an important insight into the internal working mechanisms of the photosynthetic aggregate since the results of the modeling are rather successful. Some issues concerning the resultant background charge distribution of the complex are summarized here.

The atomic partial charges approximating electrostatic potentials of the ground and excited states and the Q_y transition potential of the BChl *a* are calculated for planar molecules,[27] whereas it is known from structural data[9,10] that BChl molecules are rather distorted within the complex. However, it has been shown in ref 29 that separate calculations of atomic partial charges for different conformations of pigment molecules present in the complexes of their research do not influence the final results significantly. In addition, we have used rescaling of the calculated atomic partial charges of BChls in such a way as to obtain the expected value of the nearest neighbor excitonic coupling. We think it could at least partially compensate the possible drawback of this partial charge distribution.

In our model we used two carotenoids per protomer as comes from interpretation of X-ray diffraction,[10] even though the resolution of the second carotenoid was strongly questioned.[37] However, we treated carotenoids as background molecules only, and the influence of this second carotenoid on the site-energies of BChls is not crucial. Within our model it is possible to compensate the carotenoid effect by slightly increasing the partial charges of hydrogen-bonds to B850 ring pigments. Thus the carotenoids do not affect the overall charge distribution obtained in our simulations. Another carotenoid-related issue in our model is the normalization of the calculated atomic partial charges approximating the ground state potential of the carotenoid. Unfortunately, we could not obtain the relevant data or make any connections with the real transition dipole moment of this carotenoid in order to properly scale our calculated atomic partial charges to some observable (see the above discussion on scaling of calculated atomic partial charges of BChl *a* molecules). Still keeping in mind the minor influence of the carotenoids in our model, this issue is not significant.

The next topic to be discussed is related to the N-termini of the proteins. In our resultant background charge layout, we assumed that the amine terminal group of the α-protein is protonated and positively charged (it is responsible for a blue-shift of the B800 ring pigments from B850 ones). However, within the LH2 complex under research, the methionine N-terminus of α-proteins is modified by the carboxyl group, forming *N*-carboxymethionine.[10] While the positively charged state is necessary for spectroscopy simulations, it is unknown whether this secondary amine could be protonated. This issue is one of our future research topics.

One of the most important assumptions from our viewpoint is that the side-chain of the only arginine residue within a protomer must be deprotonated and neutral. Otherwise it produces a red-shift of the site- energies of B800 pigments of

dx.doi.org/10.1021/jp302817p | J. Phys. Chem. B 2012, 116, 7803–7814

nearly 700 cm^{-1} compared to B850 ones, and we could not find any way to compensate it within our model. It is seen from the structural data[10] that the arginine is located on the very surface of the complex pointing outward (see Figure 1). If the same structure is preserved in vivo, this side-chain would be turned into the membrane close to the cytoplasmic side. There is another charged side-chain of the same protein positioned near the discussed β-Arg20 amino acid residue, namely, negative β-Asp17, also pointing outward from the complex. However, modeling shows that only the arginine side-chain is at such a crucial position to produce an extreme site-energy shift. The positive charge of protonated arginine is carried partially by the same atoms marked NH2 and NE that are listed in ref 10 as hydrogen-bond donors to B800 BChl OBB atom (see Figure 2a). Additionally, the positive charge of arginine is approximately in the direction of the dipole moment of the Q_y transition and is situated in close proximity. Thus we found no other way to reproduce the experimental spectra as to model the side-chain of the arginine to be deprotonated and neutral.

In the present research, hydrogen-bonds are used as parameters to fine-tune the calculated LH2 absorption spectra in agreement with the experiment. Thus we restricted ourselves to a rather simple model of the hydrogen-bond-induced charge polarization, involving only two atoms of the bond donor, one of which is the hydrogen. It is the only place in our approach where we involve the hydrogen atoms (the details are presented earlier in the text). Two of the hydrogen-bond donors to B850 pigments are amino-acids with aromatic side groups, namely, tyrosine with its phenyl ring and tryptophan containing an indole ring. Another hydrogen-bond donor to B800 molecules is the arginine side-chain with different charge polarization characteristics than the mentioned aromatic side groups. Thus we assume that partial charges representing hydrogen-bonging in our model are different for different types of bond donors. For example, in the case of substituted phenols participating in hydrogen-bonding, as published in ref 45, the partial charge of the hydrogen atom is as large as 0.439*e*, whereas much smaller values of ≈0.01−0.03*e* are calculated for hydrogen charges in formamide−water and guanidinium−acetate bonded complexes.[46] These give us quite a wide range of trial values for hydrogen-bond modeling.

The hydrogen-bonds of the tyrosine and tryptophan side-chains to the BChl molecules of B850 ring are thought to play an important role in the structure of the LH2 complex (see, for example, the review of ref 4). The research involving site directed mutagenesis, optical spectroscopy, resonance Raman spectroscopy, and modeling of purple bacteria *Rhodobacter sphaeroides*[57−59] showed that replacing the hydrogen-bond donors to B850 pigments by other amino acids induces the blue-shift of the B850 band of absorption spectra up to 26 nm at 77 K. However, this shift is caused by both the structural and hydrogen-bonding changes when the residues are replaced within the pigment−protein complex. So the values of the site-energy shifts of ≈70−100 cm^{-1} produced by hydrogen-bonds to B850 ring pigments we used in our models seem rather reasonable.

The detergent molecules and water molecules presented in the structural data file[10] have been ignored in our model. It is known that in some other photosynthetic complexes, water molecules are ligands to Mg atoms of some pigments, but that is not the case for the LH2 complex under investigation. The possible electrostatic effects of the polar groups of amino acid side-chains are not taken into account, since we do not model hydrogen atoms explicitly. However, according to the lists of the close contacts between apoproteins and bacteriochlorins in ref 9, there are no such polar groups in the vicinity of B850 pigments except for considered hydrogen-bond donors, and only one polar side-chain of the residue α-Gln3 close to the B800 pigment. Thus we assume that this issue should not make essential differences in our results.

In conclusion, we have obtained exciton parameters of the LH2 aggregate from the microscopic model. The model allows us to propose several possible background charge patterns. Simulations of spectroscopy signals enable us to resolve the ambiguity and to identify the most probable charge configuration of protein side-chains as well as to identify the most probable exciton Hamiltonian.

■ ASSOCIATED CONTENT

Supporting Information

The atomic partial charges for the ground state of the carotenoid rhodopin glucoside calculated by applying the ground-state geometry optimizations using the DFT method[40] with hybrid B3LYP functional[41] are presented. The residues RG1 401 and RG1 405 from PDB entry 1NKZ[10] were used in these calculations. This material is available free of charge via the Internet at http://pubs.acs.org/.

■ AUTHOR INFORMATION

Corresponding Author

*E-mail: olga.rancova@ff.vu.lt (O.R.); darius.abramavicius@ff.vu.lt (D.A.).

Notes

The authors declare no competing financial interest.

■ ACKNOWLEDGMENTS

This research was funded by the European Social Fund under the Global Grant Measure (No: VP1-3.1-ŠMM-07-K-01-020).

■ REFERENCES

(1) Blankenship, R. E. *Molecular Mechanisms of Photosynthesis*; Blackwell Science Ltd: Malden, MA/Oxford, U.K./Carlton, Australia, 2008; p 321.

(2) van Amerongen, H.; Valkunas, L.; van Grondelle, R. *Photosynthetic Excitons*; World Scientific: Singapore/New Jersey/London/Hong Kong, 2006; p 590.

(3) Hu, X.; Ritz, T.; Damjanovic, A.; Autenrieth, F.; Schulten, K. *Q. Rev. Biophys.* **2002**, *35*, 1−62.

(4) Cogdell, R. J.; Gall, A.; Köhler, J. *Q. Rev. Biophys.* **2006**, *39*, 227−324.

(5) Hunter, C. N., Daldal, F., Thurnauer, M. C., Beatty, J. T., Eds. *The Purple Phototrophic Bacteria; Advances in Photosynthesis and Respiration*; Springer: Dordrecht, The Netherlands, 2008; Vol. *28*; p 1013.

(6) Imhoff, J. F. *Int. J. Syst. Evol. Microbiol.* **2001**, *51*, 1863−6.

(7) Zuber, H.; Brunisholz, R. A. In *Structure and Function of Antenna Polypeptides and Chlorophyll−Protein Complexes: Principles and Variability*; Scheer, H., Ed.; The Chlorophylls; CRC: Boca Raton, FL, 1991; pp 627−703.

(8) McDermott, G.; Prince, S.; Freer, A.; Hawthornthwaite-Lawless, A.; Papiz, M.; Cogdell, R.; Isaacs, N. *Nature* **1995**, *374*, 517−521.

(9) Prince, S.; Papiz, M.; Freer, A.; McDermott, G.; Hawthornthwaite-Lawless, A.; Cogdell, R.; Isaacs, N. *J. Mol. Biol.* **1997**, *268*, 412−423.

(10) Papiz, M.; Prince, S.; Howard, T.; Cogdell, R.; Isaacs, N. *J. Mol. Biol.* **2003**, *326*, 1523−1538.

(11) Koolhaas, M. H. C.; van der Zwan, G.; van Grondelle, R. *J. Phys. Chem. B* **2000**, *104*, 4489−4502.
(12) Humphrey, W.; Dalke, A.; Schulten, K. *J. Mol. Graphics* **1996**, *14.1*, 33−38.
(13) Georgakopoulou, S.; Frese, R. N.; Johnson, E.; Koolhaas, C.; Cogdell, R. J.; van Grondelle, R.; van der Zwan, G. *Biophys. J.* **2002**, *82*, 2184−2197.
(14) Koolhaas, M. H. C.; Frese, R. N.; Fowler, G. J. S.; Bibby, T. S.; Georgakopoulou, S.; van der Zwan, G.; Hunter, C. N.; van Grondelle, R. *Biochemistry* **1998**, *37*, 4693−4698.
(15) Harel, E.; Engel, G. S. *Proc. Natl. Acad. Sci. U.S.A.* **2012**, *109*, 706−711.
(16) Zigmantas, D.; Read, E. L.; Mančal, T.; Brixner, T.; Gardiner, A. T.; Cogdell, R. J.; Fleming, G. R. *Proc. Natl. Acad. Sci. U.S.A.* **2006**, *103*, 12672−12677.
(17) Alden, R. G.; Johnson, E.; Nagarajan, V.; Parson, W. W.; Law, C. J.; Cogdell, R. G. *J. Phys. Chem. B* **1997**, *101*, 4667−4680.
(18) Krueger, B. P.; Scholes, G. D.; Fleming, G. R. *J. Phys. Chem. B* **1998**, *102*, 5378−5386.
(19) Ketelaars, M.; van Oijen, A. M.; Matsushita, M.; Köhler, J.; Schmidt, J.; Aartsma, T. J. *Biophys. J.* **2001**, *80*, 1591−1603.
(20) Koolhaas, M. H. C.; van der Zwan, G.; Frese, R. N.; van Grondelle, R. *J. Phys. Chem. B* **1997**, *101*, 7262−7270.
(21) Georgakopoulou, S.; van Grondelle, R.; van der Zwan, G. *Biophys. J.* **2004**, *87*, 3010−3022.
(22) Renger, T.; Marcus, R. A. *J. Chem. Phys.* **2002**, *116*, 9997−10019.
(23) Urboniene, V.; Vrublevskaja, O.; Trinkunas, G.; Gall, A.; Robert, B.; Valkunas, L. *Biophys. J.* **2007**, *93*, 2188−2198.
(24) May, V.; Kühn, O. *Charge and Energy Transfer Dynamics in Molecular Systems*; Wiley-VCH Verlag GmbH & Co. KGaA: Weinheim, Germany, 2011; p 562.
(25) Abramavicius, D.; Palmieri, B.; Mukamel, S. *Chem. Phys.* **2009**, *357*, 79−84.
(26) Adolphs, J.; Renger, T. *Biophys. J.* **2006**, *91*, 2778−2797.
(27) Madjet, M. E.; Abdurahman, A.; Renger, T. *J. Phys. Chem. B* **2006**, *110*, 17268−17281.
(28) Müh, F.; Madjet, M. E.; Adolphs, J.; Abdurahman, A.; Rabenstein, B.; Ishikita, H.; Knapp, E.-W.; Renger, T. *Proc. Natl. Acad. Sci. U.S.A.* **2007**, *104*, 16862−16867.
(29) Adolphs, J.; Müh, F.; Madjet, M. E.; Renger, T. *Photosynth. Res.* **2008**, *95*, 197−209.
(30) Tronrud, D.; Wen, J.; Gay, L.; Blankenship, R. *Photosynth. Res.* **2009**, *100*, 79−87.
(31) Adolphs, J.; Müh, F.; Madjet, M. E.; am Busch, M. S.; Renger, T. *J. Am. Chem. Soc.* **2010**, *132*, 3331−3343.
(32) Müh, F.; Madjet, M. E.; Renger, T. *J. Phys. Chem. B* **2010**, *114*, 13517−13535.
(33) Bashford, D.; Gerwert, K. *J. Mol. Biol.* **1992**, *224*, 473−486.
(34) Gilson, M. K. *Proteins: Struct., Funct. Bioinf.* **1993**, *15*, 266−282.
(35) Abramavicius, D.; Palmieri, B.; Voronine, D. V.; Šanda, F.; Mukamel, S. *Chem. Rev.* **2009**, *109*, 2350−2408.
(36) Renger, T. *Photosynth. Res.* **2009**, *102*, 471−485.
(37) Gall, A.; Gardiner, A. T.; Cogdell, R. J.; Robert, B. *FEBS Lett.* **2006**, *580*, 3841−3844.
(38) Knox, R. S.; Spring, B. Q. *Photochem. Photobiol.* **2003**, *77*, 497−501.
(39) Olbrich, C.; Kleinekathöfer, U. *J. Phys. Chem. B* **2010**, *114*, 12427−12437.
(40) Parr, R. G.; Yang, W. *Density-Functional Theory of Atoms and Molecules*; Oxford University Press: Oxford, U.K., 1989.
(41) Becke, A. D. *J. Chem. Phys.* **1993**, *98*, 5648−5.
(42) Frisch, M. J.; Trucks, G. W.; Schlegel, H. B.; Scuseria, G. E.; Robb, M. A.; Cheeseman, J. R.; Montgomery, J. A., Jr.; Vreven, T.; Kudin, K. N.; Burant, J. C.; et al., *Gaussian 03* Revision D.01; Gaussian, Inc.: Wallingford, CT, 2004
(43) Singh, U. C.; Kollman, P. A. *J. Comput. Chem.* **1984**, *5*, 129−145.
(44) R.Gunner, M.; Saleh, M. A.; Cross, E.; ud Doula, A.; Wise, M. *Biophys. J.* **2000**, *78*, 1126−1144.
(45) Jorgensen, W. L.; Jensen, K. P.; Alexandrova, A. N. *J. Chem. Theory Comput.* **2007**, *3*, 1987−1992.
(46) Senthilkumar, K.; Mujika, J. I.; Ranaghan, K. E.; Manby, F. R.; Mulholland, A. J.; Harvey, J. N. *J. R. Soc. Interface* **2008**, *5*, 207−216.
(47) Warshel, A.; Russell, S. T.; Churg, A. K. *Proc. Natl. Acad. Sci. U.S.A.* **1984**, *81*, 4785−4789.
(48) Scholes, G.; Curutchet, C.; Mennucci, B.; Cammi, R.; Tomasi, J. *J. Phys. Chem. B* **2007**, *111*, 6978−6982.
(49) Curutchet, C.; Scholes, G.; Mennucci, B.; Cammi, R. *J. Phys. Chem. B* **2007**, *111*, 13253−13265.
(50) Renger, T.; Müh, F. *Photosynth. Res.* **2012**, *111*, 47−52.
(51) Matthew, J. B. *Annu. Rev. Biophys. Biophys. Chem.* **1985**, *14*, 387−417.
(52) Haynes, W. M., Ed. *CRC Handbook of Chemistry and Physics*; CRC Press: Boca Raton, FL, 2010; p 2610.
(53) Alia; Matysik, J.; Erkelens, C.; Hulsbergen, F.; Gast, P.; Lugtenburg, J.; de Groot, H. *Chem. Phys. Lett.* **2000**, *330*, 325−330.
(54) Abramavicius, D.; Butkus, V.; Valkunas, L. Interplay of Exciton Coherence and Dissipation in Molecular Aggregates. In *Quantum Efficiency in Complex Systems, Part II: From Molecular Aggregates to Organic Solar Cells*; Würfel, U., Thorwart, M., Weber, E. R., Eds.; Semiconductors and Semimetals; Academic Press/Elsevier: San Diego, CA, 2011; Vol. *85*; pp 3−46.
(55) Berova, N., Nakanishi, K., Woody, R. W., Eds. *Circular Dichroism: Principles and Applications*; Wiley-VCH Verlag GmbH & Co. KGaA: Weinheim, Germany, 2000; p 912.
(56) Abramavicius, D.; Mukamel, S. *J. Chem. Phys.* **2006**, *124*, 034113−17.
(57) Fowler, G. J. S.; Visschers, R. W.; Grief, G. G.; van Grondelle, R.; Hunter, C. N. *Nature* **1992**, *355*, 848−850.
(58) Fowler, G. J. S.; Sockalingum, G. D.; Robert, B.; Hunter, C. N. *Biochem. J.* **1994**, *299*, 695−700.
(59) Uyeda, G.; Williams, J. C.; Roman, M.; Mattioli, T. A.; Allen, J. P. *Biochemistry* **2010**, *49*, 1146−1159.